ELSEVIER

Materials Science and Engineering A282 (2000) 193–202

MATERIALS SCIENCE & ENGINEERING A

www.elsevier.com/locate/msea

Deformation and fracture of Al_2O_3/Al–Zn–Mg–Cu metal matrix composites at room and elevated temperatures

Yan-Lin Wu [a], Chuen-Guang Chao [b,*]

[a] *Chinamotor Company, Yangmei, Taiwan, ROC*

[b] *Department of Materials Science and Engineering, National Chiao Tung University, 1001 Ta Hsueh Road, Hsinchu, 30049 Taiwan, ROC*

Received 10 June 1999; received in revised form 26 October 1999

Abstract

Al_2O_3/Al–Zn–Mg–Cu metal matrix composites containing 2.22 ~ 3.08 wt.% Mg in the matrix alloys have been fabricated by squeeze casting. The aim of the present study is to investigate the deformation and fracture behavior of the composites at RT (room temperature) and elevated temperature. Optical microscopy, scanning electron microscopy and image analysis were used to examine and to analyze the details of the microstructure and the fracture surface. Tensile tests were utilized to evaluate the mechanical properties from 25 to 400°C. The yield stress (YS) values and UTS values for all the composites were larger than those of monolithic alloys. The UTS values for composites and monolithic alloys increased with increasing Mg content. Elevated temperature tests indicated a good strength retention for the composites; especially, UTS values of the composites showed an improvement of 18% exceeds that of the monolithic alloys from 200 to 300°C. Significant dynamic strain aging occurred for composites; however, recovery and softening remained the dominant process for monolithic alloys in the range 25–300°C.

Keywords: Ai_2O_3/Al–Zn–Mg–Cu; Dynamic strain aging; Fracture

1. Introduction

Over the past several decades extensive research developments in the field of materials science have been carried out with fiber reinforced matrix composites leading to a wide range of practical application. The fiber reinforced matrix composites, usually offer many advantages in applications where low density, high strength, high wear resistance, and high stiffness are of prime concern. It is well known that a short-fiber-reinforced aluminum composite was successfully applied to the diesel piston by Toyota in 1983 [1]. This composite showed excellent wear resistance against cast iron, good thermal conductivity, and high strength at elevated temperatures [1,2]. Most of the alloys that were employed as matrices in MMCs are light alloys, particularly those based on aluminum. These matrix alloys have included both non-heat-treatable and heat-treatable alloys. The heat-treatable alloys such as 2, 6, and 7xxx constitute a metallurgically 'active' component of the MMC whose properties can be deliberately altered to influence the properties of the final composit [3–5]. However, designing the composite microstructure and aging treatments, so that they are based directly on the precipitation characteristics of unreinforced matrix material, may impair strengthening without fully utilizing the potentiality of the composite material. It was observed that the kinetics are enhanced or retarded by reinforcing the matrix alloy during a heat treatment in difference MMC materials. Nieh and Karlak [6] found an accelerated aging effect owing to B_4C reinforcements in a 6061 aluminum alloy matrix. They suggested that the accelerated aging is primarily owing to the high dislocation density generated from thermal mismatch between the B_4C reinforcements and the aluminum matrix, and the presence of high diffusive interface in the composites. On the contrary, Ceresara and Fiorini reported that the suppression of Guinier–Preston (GP) zone formation was observed in sintered aluminum powder (SAP) type Al–Cu/Al_2O_3 [7] and Al–Mg–Si/

* Corresponding author. Tel: +886-3-573-1809; fax: +886-3-5724727.

E-mail address: t7819@cc.nctu.edu.tw (C.-G. Chao)

0921-5093/00/$ - see front matter
PII: S0921-5093(99)00762-5

Al_2O_3 [8]. The most probable reason of such a phenomenon was suggested to be the lack of quenched-in vacancies following the solution treatment, due to the availability of a large number of vacancy sinks at reinforcement-matrix interfaces. Friend and Luxton [9] indicated that the fiber array has a considerable effect on the aging-hardening response of the matrix alloy in MMCs, causing suppression on GP zone formation, which inhibits natural and artificial aging. In addition, our previous studies [10,11] also showed that higher magnesium content induced a larger amount of GP zones and η' phase formation, resulting increasing microhardness and UTS of Al_2O_3/Al–Zn–Mg–Cu composite at room temperature (RT).

Serrated yielding, or the Portevin–Le Chatelier, effect has been observed in a large number of alloy systems, including steels [12,13], aluminum alloys [14,15], nickel-base materials [16], and so on. The effect is generally attributed to a dynamic strain aging process which occurs when solute atoms are diffusing sufficiently rapidly to slow down dislocations, moving under the action of an applied stress by forming 'atmospheres' around them. If the solutes are interstitial, for example C and N in b.c.c. iron, serrated yielding may be observed in tests carried out at temperatures close to RT. For substitutional solutes the effects are normally seen only at elevated temperatures, unless diffusion has been artificially accelerated for example: by quenching from a high temperature to retain excess vacancies; by generating vacancies during plastic deformation; or by radiation damage. N. Chung and his coworker [17] reported that the occurrence of shear bands and catastrophic, low-strain fracture in 7075 Al–Zn–Mg–Cu alloy was associated with negative strain-rate sensitivity of the flow stress and exhibited serrated stress–strain curves. Because the precipitation and dynamic strain aging in Al_2O_3/Al–Zn–Mg–Cu composites with various magnesium contents, especially at high temperature tensile test, may be complicated and have not been fully characterized before, the purpose of this study was to compare the dynamic strain aging characteristics and to investigate fracture behavior of the composites with various magnesium by studying their tensile properties in the range 25–400°C.

Table 1
Composition of the matrix alloys

Heat no.	Mg (wt.%)	Zn (wt.%)	Cu (wt.%)	Al (wt.%)
Heat 1	3.08	5.17	1.25	Balance
Heat 2	2.70	5.20	1.24	Balance
Heat 3	2.22	5.15	1.22	Balance

2. Experimental procedure

Squeeze casting produced the composite materials. The aluminum matrix alloys were prepared to contain 2.22, 2.70 and 3.08 wt.% Mg, respectively, by melting 7075 Al and Al-10 wt.% Mg master alloy. The composition of the Al-10 wt.% Mg is 10.06 wt.% Mg, 0.01 wt.% Fe and 0.03 wt.% Si. The chemical compositions of the matrix alloys analyzed by inductively coupled plasma-mass spectrometer (ICP-MS) are listed in Table 1.

The basis of the fabrication technique has been described in our previous study [10]. SAFFIL Al_2O_3 short fibers (3 μm in diameter) were fabricated into a $20 \times 18 \times 100$ mm^3 preform block by press forming. In this case, short fibers were mixed homogenously with water, accompanied by a small addition of binder (SiO_2 nH_2O). During press forming, the slurry was poured into the mold, and dewatering was conducted while the final preform was shape. The fiber volume fraction (V_f) of each composite was 0.1. The preform was preheated at 700°C and introduced in the mold which was preheated to 450°C. The liquid aluminum alloy at 780°C was squeezed into fiber preform by a 40 MPa hydraulic press to form the composites.

Using light microscopy and scanning electron microscopy (SEM) carried out microstructural characteristization. Tensile specimens were cut out from the casting as a gauge length of 13 mm with a cross section of 4×2 mm^2. Specimens were solution treated at 480°C for 48 h, then quenched into water. Aging of composites was carried out in an oil bath at 120°C for 24 h while aging of monolithic alloys was at 120°C for 72 h. The peak aging treatment was decided by prior optimization of matrix microhardness in the base alloy and the composites [10,11]. Tensile tests were carried out with an Instron tensile test machine at temperature ranging from 25 to 400°C, with a strain rate of 2.3×10^{-4} s^{-1}. Each specimen was kept for 10 min to ensure uniformity in the test temperature which was monitored to accuracy of ± 3°C. A Vickers microhardness measurement on the matrix (between fibers) of tensile tested specimens was made using a diamond pyramid indenter and 50 g load and one was excluded as the value was extremely higher to avoid influence of microhardness by the fibers on the measurement. At least ten hardness measurements were made for each tested condition to ensure accurate results. SEM examined the fracture surfaces.

3. Results

3.1. Microstructure

Fig. 1 shows a 3-D light micrograph of the composite. The fibers are randomly distributed in the com-

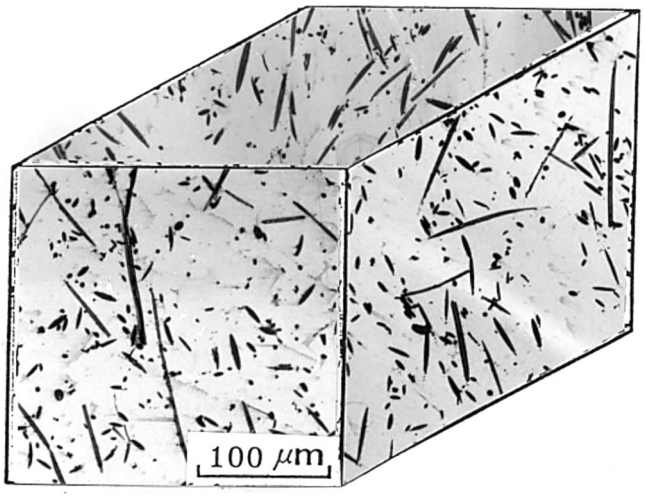

Fig. 1. 3-D light micrograph of the composite.

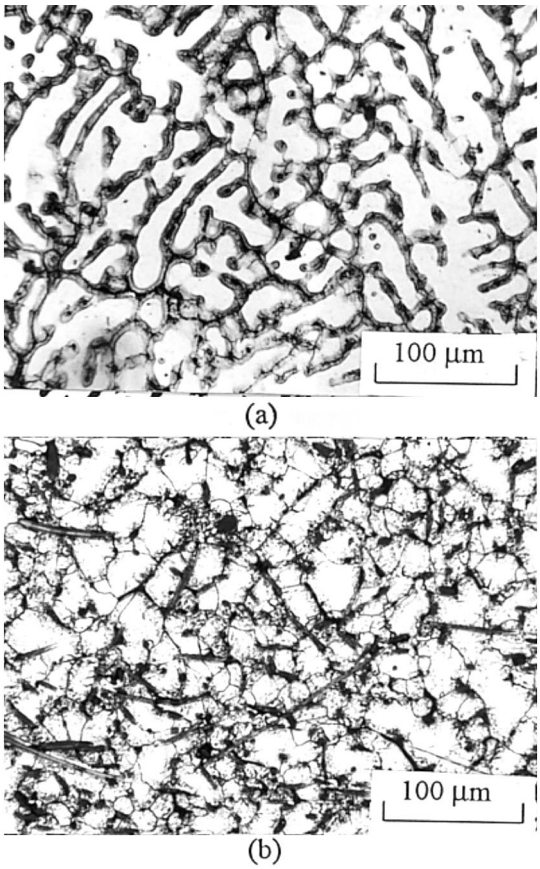

Fig. 2. Etched light micrographs of the as-cast materials (a) monolithic alloy (2.22 wt.% Mg) (b) 0.1 V_f composite.

posite. Fig. 2 shows an etched light micrograph of heat 3 in Table 1 for the as-cast condition (a) the monolithic alloy and (b) the composite. Segregation can not be avoided in both the monolithic alloy and the composite. The dendrite arm spacing of the composite (about 13 μm) is smaller than that of the monolithic alloys (about 20 μm). It is suggested that Al_2O_3 fibers acted as obstacles during solidification. Fig. 3 shows typical micrographs of solution-treatment materials. The segregation and dendrite structure are nearly eliminated by solution treatment in the composite but exist in 7075 Al.

3.2. Elevated temperatures properties

The relationship between tensile properties of composites with various Mg and test temperature is shown in Fig. 4. Serrated flow is exhibited by the composites at temperature between RT and 200°C. Some serrated flow is found even at the lower test temperature, 25°C, although its extent is very limited, consisting of only a few serrations in the stress–strain curve. The stress–strain curve is sometimes characterized by successive, regularly spaced load drops of a saw-tooth nature (fine serrations), especially at 100°C. At higher temperature 200°C the appearance of the serrations increases in size somewhat different from those at 100°C. Comparison of the flow curves in Fig. 4 indicates an increase in work hardening rate with increasing magnesium content below 200°C. The monolithic alloys have the same trend shown in Fig. 5. However, serrations are ob-

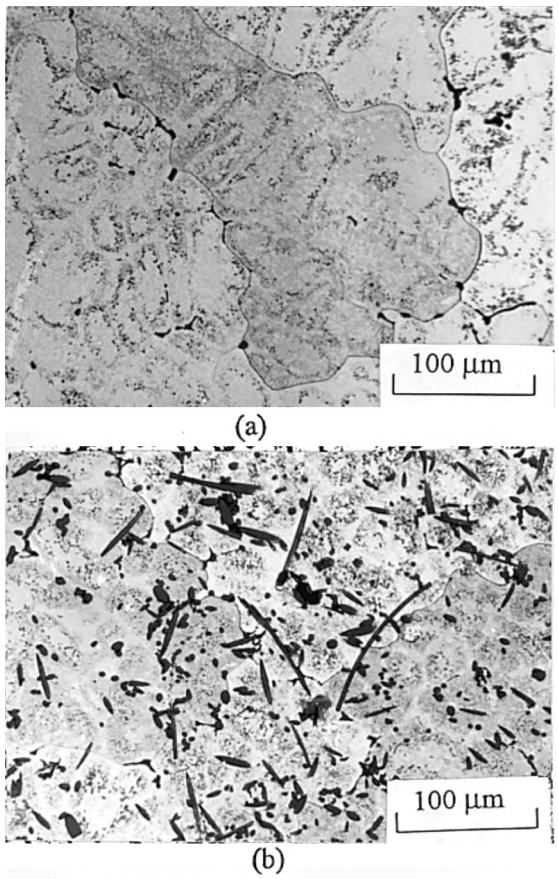

Fig. 3. Etched light micrographs of the solution-treated materials (a) monolithic alloy (2.22 wt.% Mg) (b) 0.1 V_f composite.

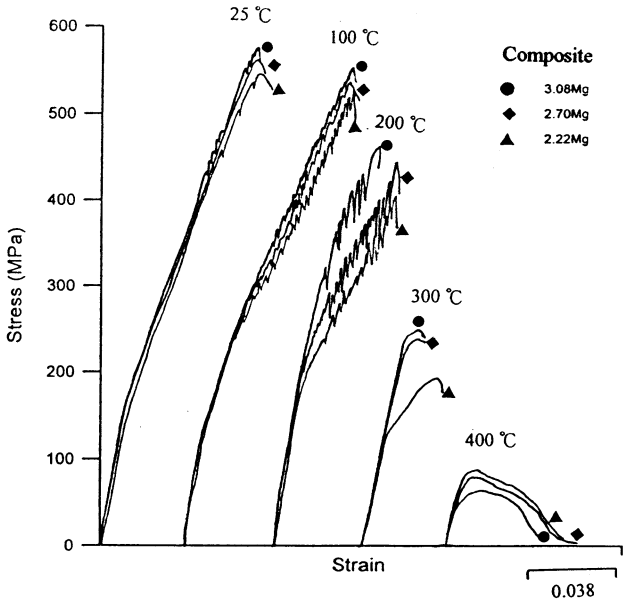

Fig. 4. Stress–strain curves of composites at temperature between 25 and 400°C.

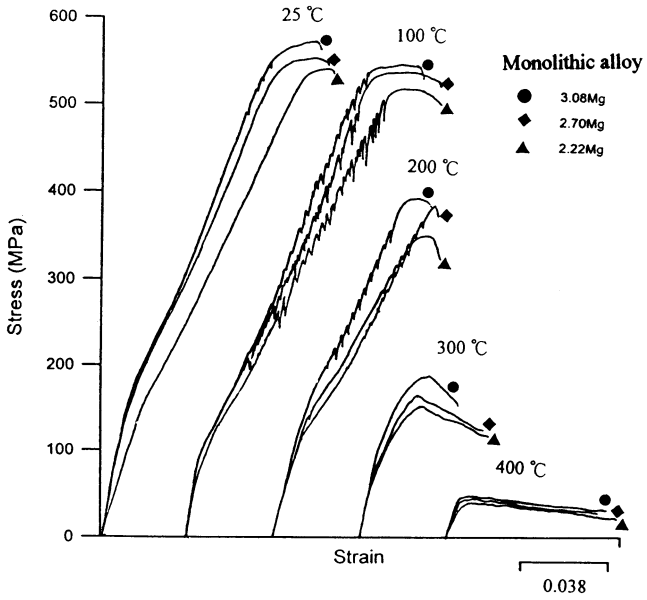

Fig. 5. Stress–strain curves of monolithic alloys at temperature between 25 and 400°C.

served only on the stress–strain curve of monolithic alloy with 3.08 wt.% Mg at RT; for alloys with 2.22 and 2.70 wt.% Mg the curves are almost completely smooth. Fig. 6 illustrates the yield stress (YS) variation for monolithic alloys and for the composites at different temperatures. YS values of composites are higher than that of the base alloy at all temperatures. At RT the composite containing 3.08 wt.% Mg exhibits the highest UTS value. Table 2 represents the percentage ratio of UTS for the materials at different temperatures to the composite (containing 3.08 wt.% Mg) strength at RT ($\sigma/(\sigma_c)$RT $\times$ 100). It can be inferred from these values that composite have good strength retention at temperature up to 300°C. However, at 400°C the composites exhibit a drastic decrease in UTS retention, although UTS values of composites are still higher than one of monolithic alloys. Fig. 7 shows the elongation variation for monolithic alloys and composites at different temperatures. Fig. 7(a) shows the elongation of monolithic alloys is almost the same with various magnesium below 200°C. However, the elongation obvi-

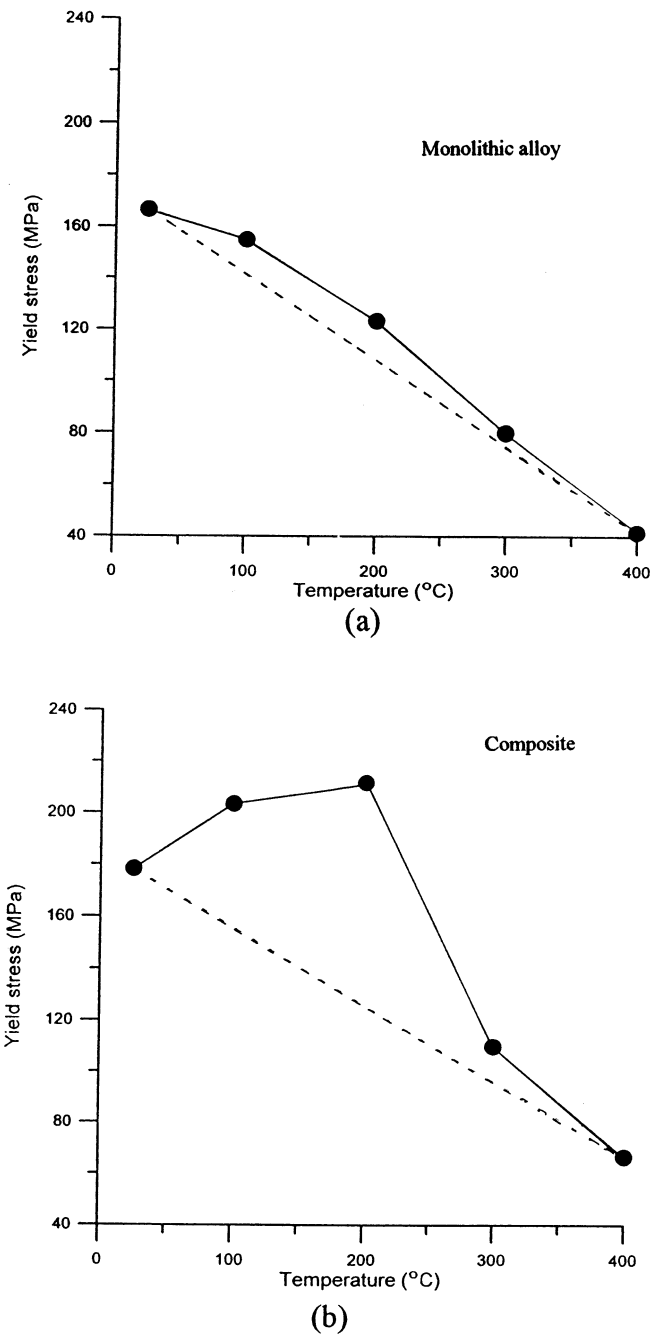

Fig. 6. Yield stress variation for (a) monolithic alloy (2.22 wt.% Mg) (b) composite at different temperatures.

Table 2
The percentage ratio of UTS for the materials at different temperatures to the composite (containing 3.08 wt.%Mg) strength at RT $(\sigma/(\sigma_c)_{RT} \times 100)$

Mg content	Temperature materials	25°C	100°C	200°C	300°C	400°C
3.08 wt% Mg	MMC	100.0	95.8	79.8	43.3	11.7
	7075 Al	98.3	95.9	67.5	32.8	7.7
2.70 wt% Mg	MMC	96.4	92.7	76.0	43.0	16.0
	7075 Al	96.2	91.5	65.9	28.1	8.1
2.22 wt% Mg	MMC	94.0	90.0	72.0	33.6	14.4
	7075 Al	93.7	89.0	60.2	27.4	8.7

ously increases with decreasing magnesium at 400°C. The elongation of the composites at all test temperatures is almost the same value in various magnesium samples shown in Fig. 7 (b).

3.3. Fractography

Fig. 8 shows micrographs taken from the neighborhood of fracture position of monolithic alloys after tensile test at different temperatures. The fractures along the interdendritic segregation at lower temperatures (below 300°C) are obviously observed in Fig. 8(a) and (b). The deformed grains and necking at the fracture over 300°C are observed in Fig. 8(c). Fig. 9 shows the micrograph taken from the neighborhood of fracture position of composites after tensile test at different temperatures. The fracture is not along the interdendritic segregation because the segregation is eliminated in composites (Fig. 3) by solution treatment. In addition, deformation in the composites is limited at all temperatures as revealed by flat fractures unlike the unreinforced alloy which exhibited necking at elevated temperatures. Fig. 10 shows SEM fractograph of fracture surfaces of monolithic alloys. On testing at temperatures between 25 and 200°C the monolithic alloys produce dimples mixed with intergranular (interdendritic segregation area) fracture surfaces shown in Fig. 10. The fracture surfaces become dimpled above 200°C shown in Fig. 10(b). Fig. 11 shows SEM fractograph of fracture surfaces of composites. The fracture surface of the sample exhibits many broken fibers as shown in Fig. 11(b). The failures produced in composites in the range 100–200°C are essentially similar to those at RT. However, the fracture surface of the sample tested at 300°C exhibits many voids near fibers. In addition, the fracture surface of the sample tested at 400°C exhibits a rougher surface on the fibers shown in Fig. 11(d). It means that at first, plastic deformation of the matrix occurs in tensile tests and then the fiber separates from the matrix above 200°C.

3.4. Microhardness

Fig. 12 shows the room temperautre microhardness variation for monolithic alloys and composites upon annealing at 200 and 300°C. The microhardness is almost the same within 50 min for all the samples at 200°C, since the precipitation is still not overaged. However, the microhardness drastically decreases over 10 min for all the samples at 300°C, because the precipitation is overaged. Fig. 13 shows the microhardness tested soon after quenching for monolithic alloys and composites at various temperatures tensile test. The microhardness increases after tensile test at RT due to work hardening. However, the microhardness is almost the same after tensile test at elevated temperatures except one of composites at 300°C.

4. Discussion

Several strengthening mechanisms have been identified operating independently or concurrently in MMCs. There include quench strengthening, strengthening due to internal stresses, precipitation hardening and load sharing between the reinforcement and matrix [18–20]. In the present investigation, Table 2 lists the percentage ratio of UTS for the materials at different temperatures to the composite (containing 3.08 wt.% Mg) strength at RT $(\sigma/(\sigma_c)RT \times 100)$. The UTS values of composites are almost the same as those of monolithic alloys at tested temperature below 100°C. This may be due to the fact that the strengthening phases, GP zones and η' precipicates, are suppressed in the composites [10,11] although the fibers do provide some strengthening. In addition, the UTS value of all materials increases with increasing magnesium content. Higher magnesium content induces a larger amount of GP zones and η' phase formation, resulting in increased UTS. However, there is a drop in UTS values for all the materials as shown by Table 2 at elevated test temperature (above 100°C). This is attributed to result of reduction in matrix strength as well as a reduction in dislocation density due to diffusion annealing. The UTS values of composite with various magnesium are degraded in a range from 72.0 to 79.8% and 33.6 to 43.3% at 200 and 300°C, respectively. The UTS values

of monolithic alloys with various magnesium content are degraded in a range from 60.2 to 67.5% and 27.4 to 32.8% at 200 and 300°C, respectively. Obviously, the UTS value for composites 18% ($UTS_{(c)} - UTS_{(m)}/UTS_{(m)}$) exceeds that of the monolithic alloys at the test temperature from 200 to 300°C. It may be proposed that improved strength retention at elevated temperature can be provided a continuity of reinforcement

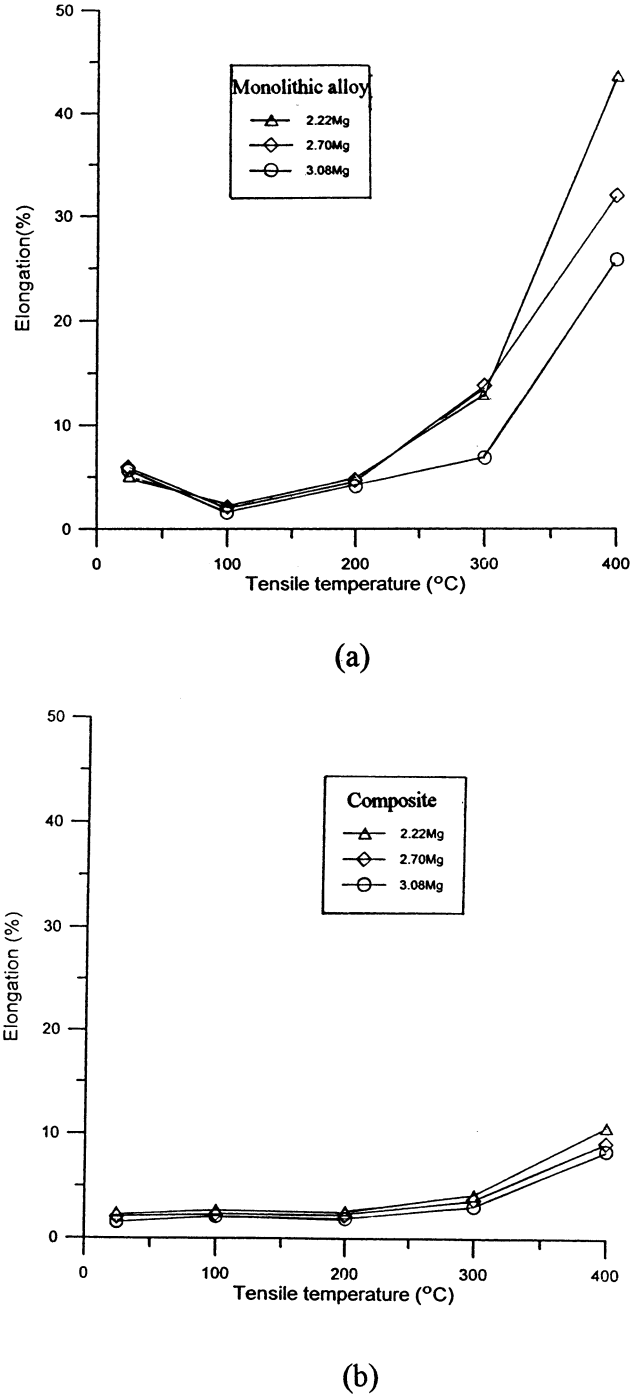

Fig. 7. Elongation of (a) monolithic alloys and (b) composites at different test temperatures.

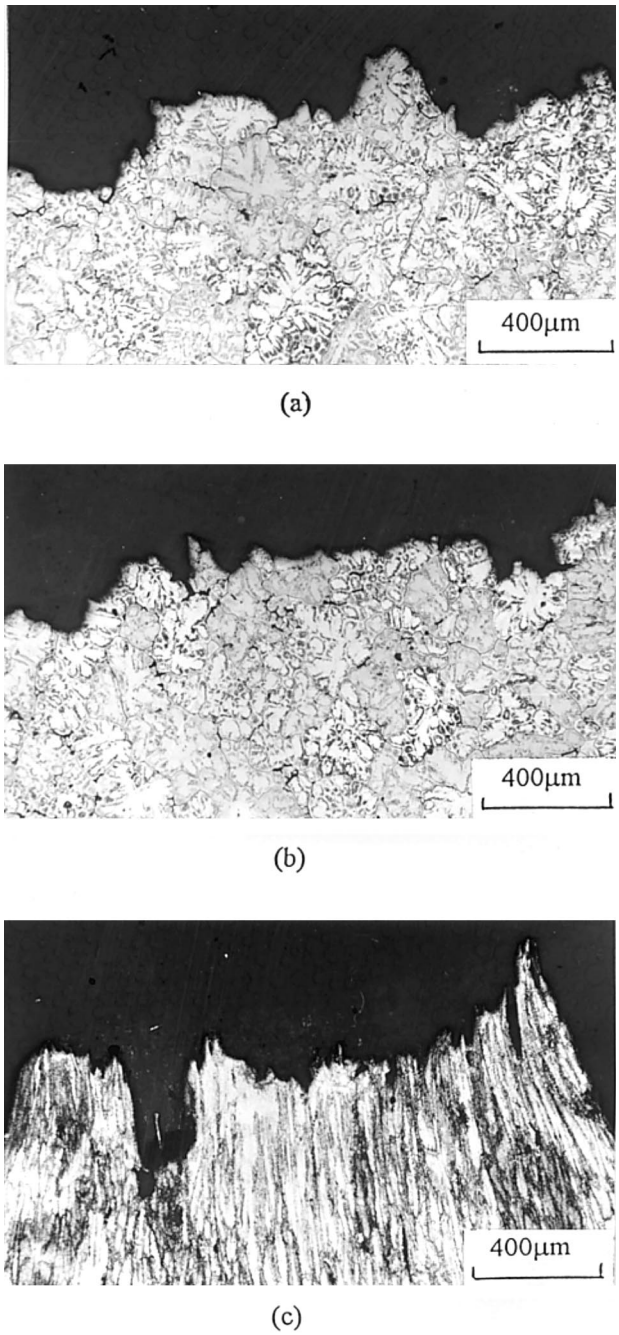

Fig. 8. Micrograph taken from the neighborhood of fracture position of monolithic alloy (2.22 wt.% Mg) after tensile test at different temperatures (a) RT (b) 100°C (c) 400°C.

medium by forming an interconnected reinforcement/matrix network [21] and be affected by dynamic strain aging.

The tensile-strain curves of both monolithic alloys and composites exhibit serration for test temperature between 25 and 200°C, and the stress levels increase with increasing magnesium contents. This behavior is characteristic of dynamic strain aging associated with

one or more of the substitutional elements (presumably Mg and Zn) in the materials. J.G. Morris [22] proposed that basically three types of flow stress-deformation temperature curves could be obtained in aluminum alloys as shown in Fig. 14. If significant dynamic strain aging occurs then curve (a) results. This curve possesses a transient in which the flow stress increases with an increase in deformation temperature. If dynamic strain aging occurs to an extent that it merely nullifies the effect of normal recovery and softening then curve (b)

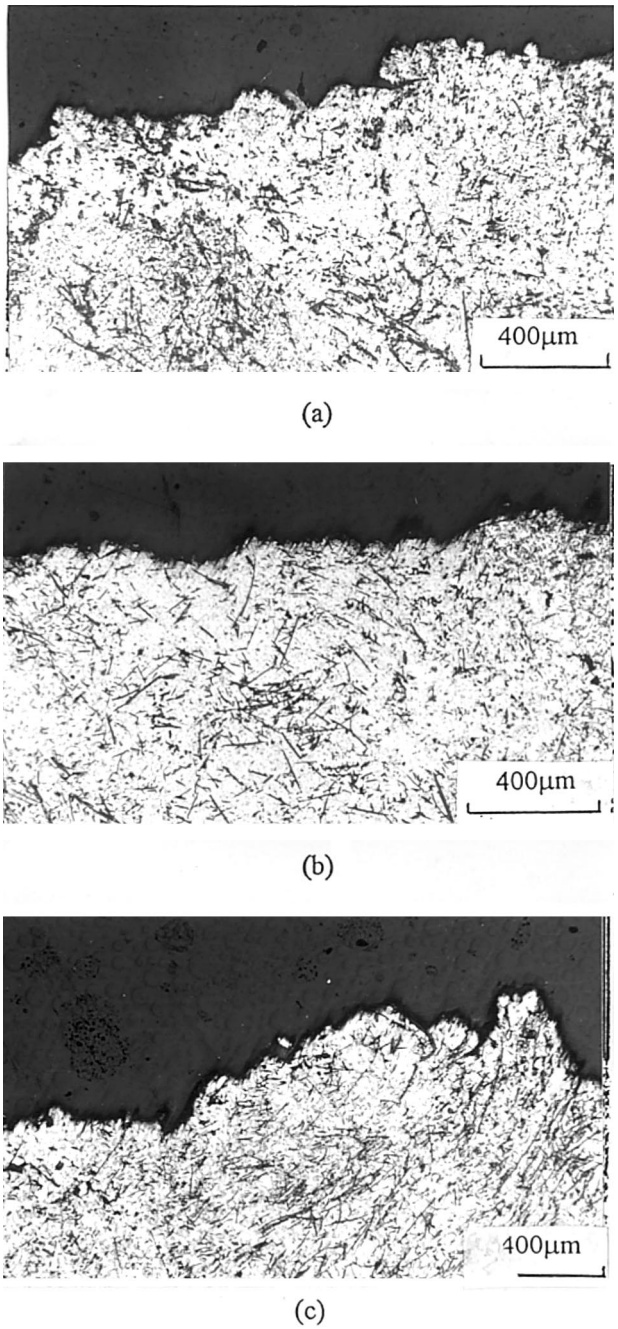

Fig. 9. Micrograph taken from the neighborhood of fracture position of composite (2.22 wt.% Mg) after tensile test at different temperatures (a) RT (b) 100°C (c) 400°C.

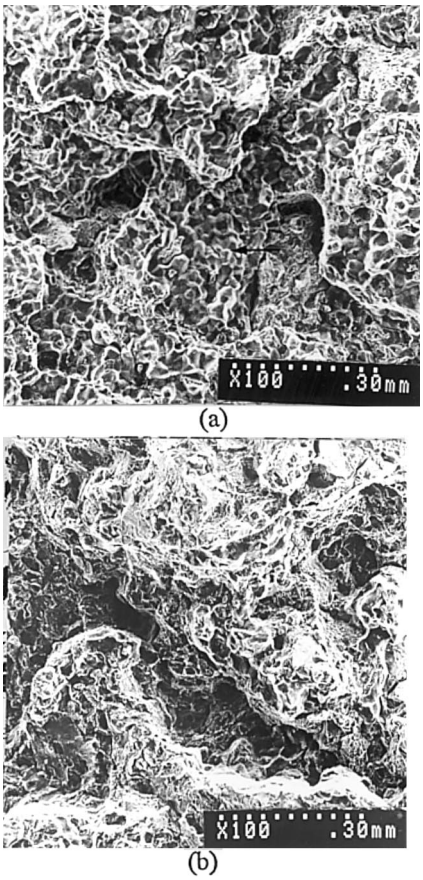

Fig. 10. SEM fractograph of fracture surfaces of monolithic alloy (2.22 wt.% Mg) at different temperatures (a) RT and (b) 400°C.

is obtained. In this case, a transient is produced in which the flow stress remains constant with an increase in deformation temperature. If dynamic strain aging occurs to a lesser degree than in either (a) or (b) then recovery and softening remain the dominant processes as the deformation temperature is increased and a transient as shown in curve (c) is produced. If no dynamic strain aging occurs then the flow stress response is as shown in (d). In this study, the flow stress-deformation temperature curve shown in Fig. 6 obviously belongs to (a) curve for the composite (Heat 3) but belongs to (c) curve for the monolithic alloy. It means that the effect of dynamic strain aging on flow stress is larger than the effect of recovery and softening on flow stress at elevated temperature for composites. However, the effect of dynamic strain aging on flow stress is smaller than the effect of recovery and softening on flow stress for monolithic alloys. The significant dynamic strain aging occurred in composites are due to the high dislocation density generated from thermal mismatch between the Al_2O_3 reinforcements and the aluminum matrix, and the presence of fibers produced obstacles for dislocation. Comparison of Fig. 12(b) and Fig. 13(b), shows that the microhardness of composite after tensile testing is much higher than that after

annealing at 300°C due to work hardening by dynamic strain aging. Comparison of the elongation at RT with those at 100 and 200°C where dynamic strain aging and serrated yielding shows that dynamic strain aging in monolithic alloys may be regarded as an embrittling effect, similar to 'Blue Brittleness' in steel.

M.D. Kulkarni etc [23] reported that the lower value in RT UTS and elongation for the 7075 Al–SiCp composites is attributed to the damage accumulation by particle fracture and the matrix-reinforcement interfaces decohesion. In this study, the fracture surface of the composite does not exhibit pullout fibers and reaction zone at interface shown in Fig. 11. It means that the bonding between the matrix and fibers is good. Therefore, the UTS value of all composites is larger than that of monolithic alloys, although the strengthening phases, GP zone and η' phase, is depressed in composites.

5. Conclusions

In our present study, the mechanical properties of Al_2O_3/Al–Zn–Mg–Cu composites containing Mg content from 2.22 to 3.08 wt.% at test temperatures from 25 to 400°C are summarized as follows:

(1) The YS values and UTS values for all the composites are larger than those of monolithic alloys. The UTS values for composites and monolithic alloys increase with increasing Mg content.

(2) Elevated temperature tests indicate a good strength retention for the composites; especially,

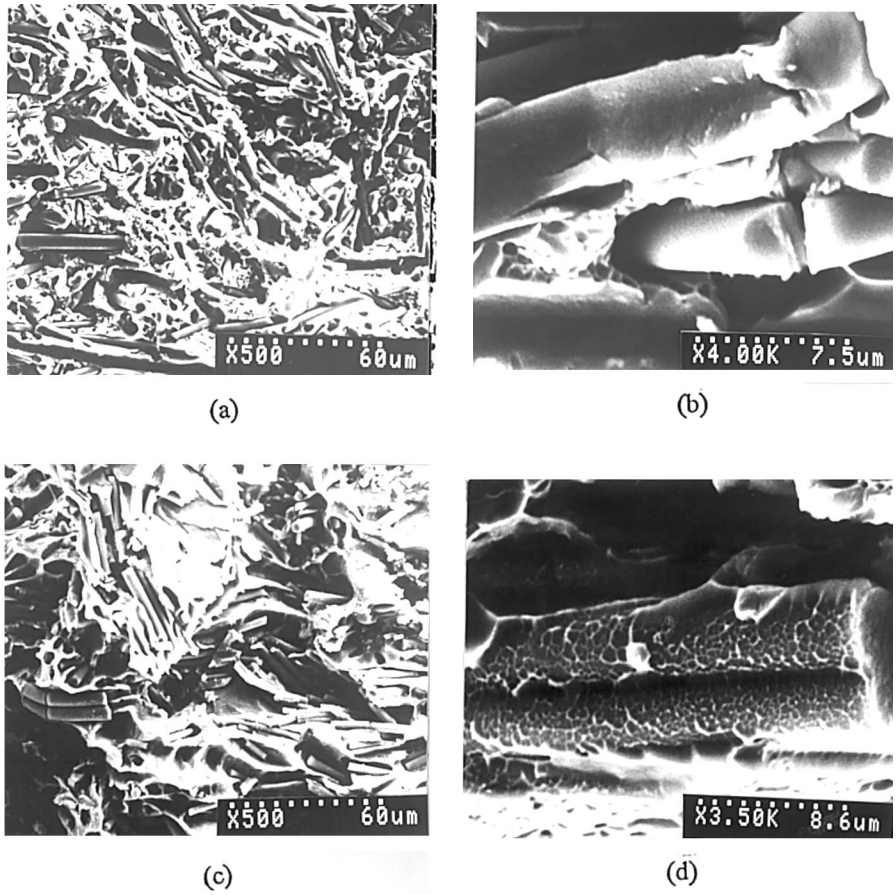

Fig. 11. SEM fractograph of fracture surfaces of composite (2.22 wt.% Mg) at different temperatures (a) R.T. (c) 400°C and enlarge area of (a), (c) respectively in (b) and (d).

U.T.S values of the composites show an improvement of 18% over those of monolithic alloys from 200 to 300°C.

(3) Significant dynamic strain aging occurs for composites, while recovery and softening remain the dominant process for monolithic alloys in the range 25 to 300°C.

(4) Tensile ductility in the composites is limited at all temperatures as revealed by flat fractures unlike the unreinforced alloy which exhibits necking at elevated temperatures (above 200°C).

Acknowledgements

The authors are pleased to acknowledge finical support of this research by the National Science Council, PR China, under Grant No. NSC86-2216-E009-012.

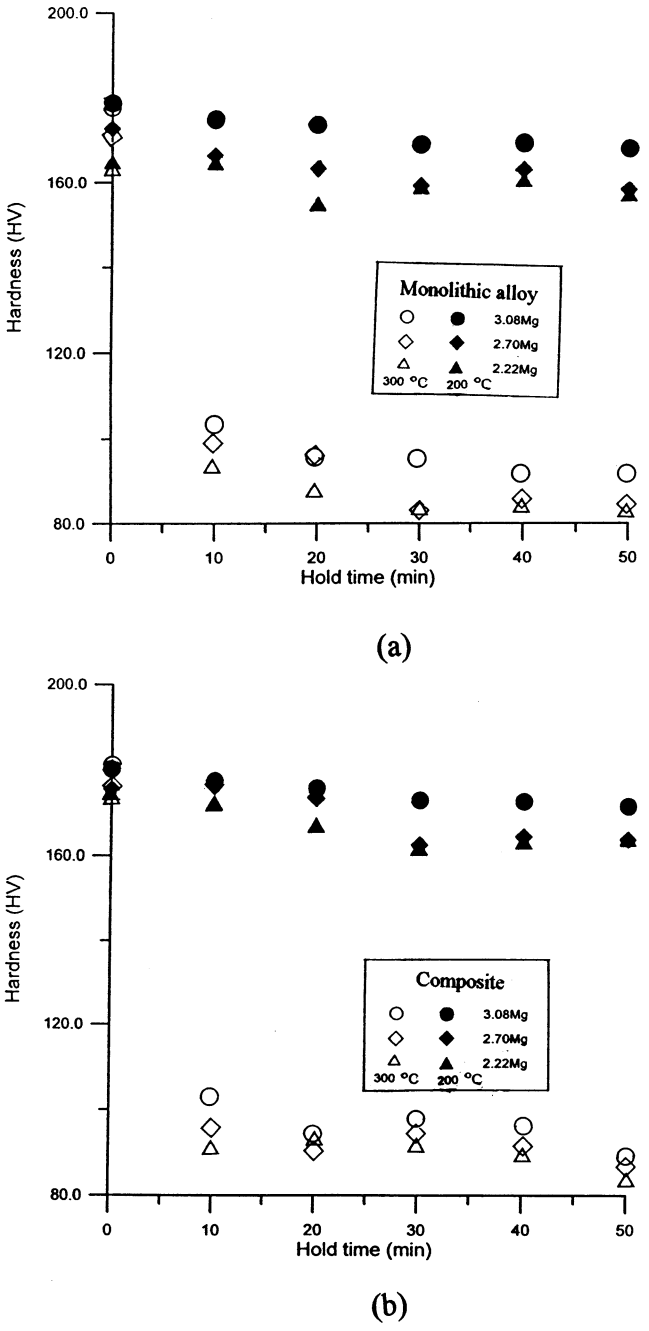

Fig. 12. Room temperature microhardness variation for (a) monolithic alloys and (b) composites after annealing at 200 and 300°C.

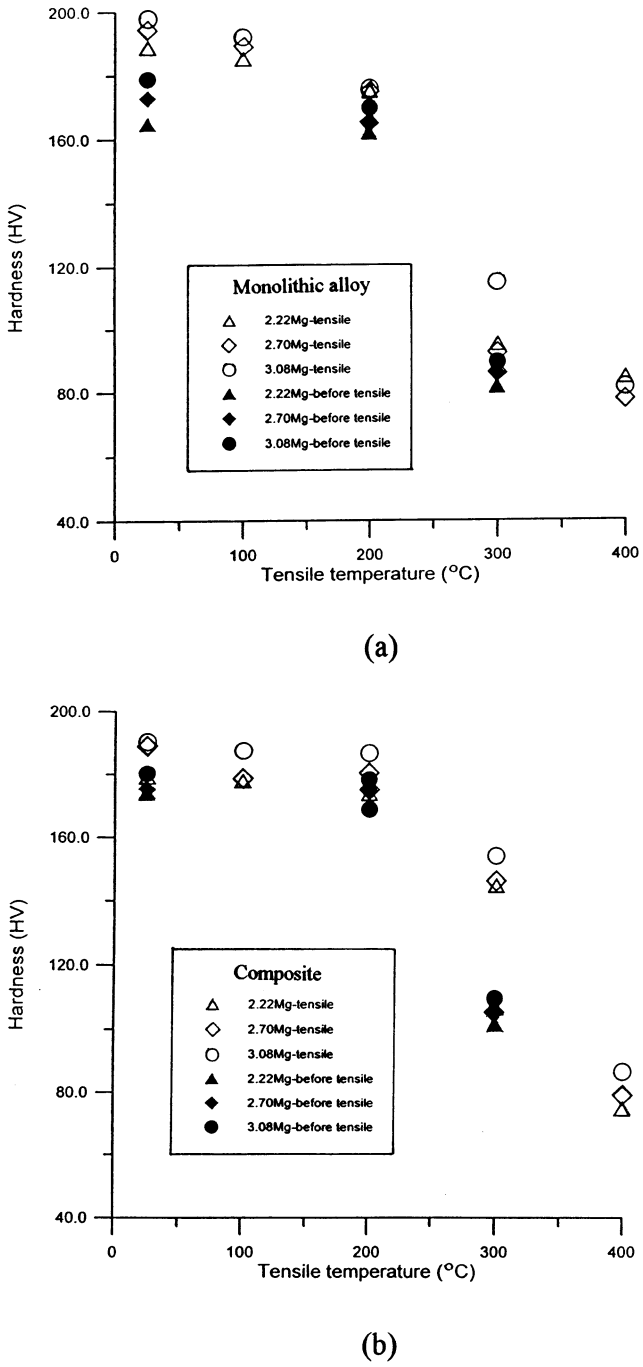

Fig. 13. Room temperature microhardness tested soon after quenching from tensile tested at 200 and 300°C for (a) monolithic alloys and (b) composites.

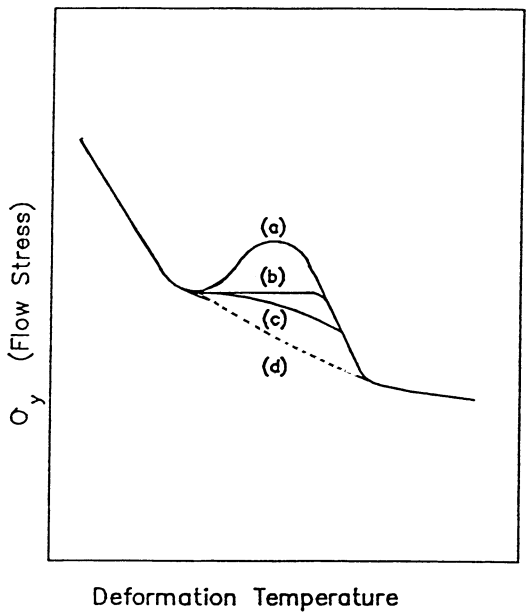

Fig. 14. Schematic flow stress-deformation temperature curves for aluminum alloys [22].

References

[1] Y. Kaneko, H. Murakami, K. Kuroda, S. Nakazaki, Found. Trade J. 148 (1980) 397.
[2] C.S. Liauo, H. Chang, J.C. Hunag, P.W. Kao, Metall. Mater. Trans. 26A (1995) 143.
[3] D. Kwon, S. Lee, B. Roh, Metall. Trans. 24A (1993) 1125.
[4] S.M. Pickard, B. Derby, Acta Metall. Mater. 38 (1990) 537.
[5] B.V.R. Bhat, Y.R. Mahajan, H.M.D. Roshan, Y.V.R.K. Prasad, Metall. Trans. 23A (1992) 2223.
[6] T.G. Nieh, R.F. Karlak, Scripta Metall. 18 (1984) 25.
[7] S. Ceresara, P. Fiorini, Powder Metall. 4 (1981) 210.
[8] S. Ceresara, P. Fiorini, Powder Metall. 1 (1979) 1.
[9] C.M. Friend, S.D. Luxton, J. Mater. Sci. 23 (1988) 3173.
[10] M.C. Chou, C.G. Chao, Metall. Trans. A26 (1995) 1035.
[11] J.H. Hsieh, C.G. Chao, Mater. Sci. Engr. A214 (1996) 133.
[12] M.S. Rashid, Metall. Trans. 7A (1976) 497.
[13] A.D. Sachdev, Metall. Trans. A13 (1982) 1793.
[14] P.R. Cetlin, A.S. Gulec, R.E. Reed-Hill, Metall. Trans. 4 (1973) 513.
[15] J.E. King, C.P. You, J.F. Knott, Acta Metall. 29 (1981) 1553.
[16] P.A. Mulford, Metall. Trans. A10 (1979) 1527.
[17] N. Chung, J.C. Embury, J.D. Evensen, N.G. Hoagland, C.M. Sargent, Atca Metall. 25 (1977) 377.
[18] W.S. Miller, M.J. Humphreys, Scripta Metall. Mater. 25 (1991) 34.
[19] T.S. Srivatsan, J. Mattingly, J. Mat. Sci. 28 (1993) 611.
[20] P. Mummery, B. Derby, Mater. Sci. Engr. A135 (1991) 221.
[21] A.G. Evans, J.W. Hutchinson, R.M. McMeekings, Scripta Metall. Mater. 25 (1991) 3.
[22] J.G. Morris, Mater. Sci. Engr. 13 (1974) 101.
[23] M.D. Kulkarni, P.S. Robi, R.C. Prasad, P. Ramakrishnan, Mater. Trans JIM 37 (3) (1996) 223.